Progress of Theoretical Physics, Vol. 128, No. 3, September 2012

A Boundary Integral SPH Formulation

— *Consistency and Applications to ISPH and WCSPH* —

Fabricio Macià, Leo M. González, Jose L. Cercos-Pita
and Antonio Souto-Iglesias

Naval Architecture Department (ETSIN), Technical University of Madrid (UPM), 28040 Madrid, Spain

(Received May 11, 2012; Revised July 17, 2012)

One of the historical problems appearing in SPH formulations is the inconsistencies coming from the inappropriate implementation of boundary conditions. In this work, this problem has been investigated; instead of using typical methodologies such as extended domains with ghost or dummy particles where severe inconsistencies are found, we included the boundary terms that naturally appear in the formulation. First, we proved that in the 1D smoothed continuum formulation, the inclusion of boundary integrals allows for a consistent $\mathcal{O}(h)$ formulation close to the boundaries. Second, we showed that the corresponding discrete version converges to a certain solution when the discretization SPH parameters tend to zero. Typical tests with the first and second derivative operators confirm that this boundary condition implementation works consistently. The 2D Poisson problem, typically used in ISPH, was also studied, obtaining consistent results. For the sake of completeness, two practical applications, namely, the duct flow and a sloshing tank, were studied with the results showing a rather good agreement with former experiments and previous results.

Subject Index: 024

§1. Introduction

The SPH scheme is a Lagrangian model based on a smoothing of the spatial differential operators of fluid-dynamics equations and on their subsequent discretization through a finite number of fluid particles. The smoothing procedure is performed at the continuum level using a compact support kernel function whose characteristic length is the smoothing length h. The resolution of the discrete SPH scheme is a function of the smoothing length h and the mean particle distance Δx. In this framework, the (continuous) equations of the fluid-dynamics should be recovered as both h and $\Delta x/h$ simultaneously tend to zero.[1] Colagrossi and Landrini[2] demonstrated that when boundaries are not present, the SPH approximation of a function $\langle u \rangle (\boldsymbol{x})$ differs $\mathcal{O}(h^2)$ from the analytical function $u(\boldsymbol{x})$. Quinlan et al.[3] studied the errors in the first-order derivatives of a classical SPH implementation and its dependence on the particle spacing and smoothing length when no boundaries were considered. In Ref. 4), this work was extended to 3D and a complete consistency study was performed for first- and second-order derivatives.

The SPH simulations in engineering usually involve solid boundary conditions (BC) for both the velocity and pressure fields. In the SPH framework, these conditions have been implemented in the past in a number of different ways: by using boundary force-type models,[5),6)] by modifying the structure of the kernel in the

neighborhood of the boundaries,[7] by creating virtual particles at the other side of the boundary through mirroring techniques[2] and by renormalizing the boundary terms that explicitly appear in the integral SPH formulation.[8–10] This latter approach is the main focus of the present work.

An incompressible fluid is one in which the density is not altered by pressure changes and the only local condition to obtain mass conservation is that of a divergence-free velocity field. Depending on how the density and incompressibility constrain are treated, different formulations can be found in the SPH literature when incompressible fluids are simulated. On the one hand, the WCSPH uses an explicit formulation where the pressure gradient and the divergence and Laplacian of the velocity field are calculated applying discrete and smoothed versions of these operators to a discretized field. Physically, the pressure plays a thermodynamic derived role through the state equation. An interesting discussion about the influence of the truncation of differential operators close to the boundaries in WCSPH can be found in Ref. 11) where a complete analysis of several formulations of the pressure gradient and velocity divergence operators is performed when an inviscid flow is considered in the presence of a free surface. These ideas were extended to the Laplacian operator in Ref. 12).

On the other hand, in the ISPH[14] and MPS[15] approximations, the zero divergence condition is enforced by solving a Poisson equation for the pressure field at every time increment. Here, the pressure acts as a Lagrange multiplier to satisfy the incompressible hypothesis. In this incompressible formulation, pressure moves as a wave that propagates with an infinite sound speed. Although no real fluid is completely incompressible, it is generally accepted that the incompressibility assumption is a good approximation when the Mach number $M = v/c < 0.3$, where v is the characteristic fluid speed and c is the speed of sound. Many techniques presented in the literature[16–19] solving the incompressible Navier-Stokes system of mass and momentum conservation are based on projection methods. This technique is often referenced in the literature as the 'fractional step', 'semi-implicit' or 'pressure-Poisson equation' method. The projection method decouples velocity and pressure by factorizing the Navier-stokes system in such a way that the system can be solved as a sequence of two simpler steps. In the first step, an intermediate velocity $\boldsymbol{u}^*$ is calculated and, in the second, this intermediate velocity is projected onto a divergence-free space, which requires the solution of a Poisson equation to obtain the pressure field p. The solution of the Poisson problem has a demonstrated consistency with the most common boundary conditions used in fluid mechanics when classical numerical methods are applied (finite elements, finite differences, finite volumes, etc...). Some contentious issues related to the boundary conditions used in the second step are easily found in the literature.

Different versions of the Laplacian operator have been used in the SPH context; for a complete review of the different versions, see Ref. 13). Another interesting discussion about this discretization is included in Ref. 14) where two different discretizations are studied; the first is an exact discretization of the Laplacian operator whilst the second is an approximation of it. It seems that some numerical inconsistencies appear when the exact formulation is used. Following the suggestion from

Ref. 20), the approximate Laplacian operator with the same form as a diffusion term is also used here.

Generally, two types of boundary conditions are used in SPH: prescribed velocity on a moving or steady wall and a constant pressure for any free surface. When the velocity is prescribed on a boundary, a homogeneous Neumann boundary condition is used for the pressure. On the other hand, when a free surface is present, a Dirichlet boundary condition is imposed to obtain a constant pressure on the boundary.

These boundary conditions are present in previous ISPH works[14),20)] where the Poisson equation was solved and the pressure was calculated. The methodology used to impose boundary conditions does not differ at all from the ones used by any other discretization methods, and in most of these cases, the presence of extra particles is necessary to satisfy the kernel completeness. Another important remark is that very few consistency tests can be found when the discretization parameters (number of particles and the smoothing length) tend to the continuous formulation. In the work performed by Macià et al.,[21)] the inconsistency evidence was presented when boundary conditions were implemented artificially extending the domain. An important improvement was achieved and described in Refs. 8), 9) and 10), where boundary integrals were used to impose the boundary conditions in a weakly compressible SPH (WCSPH) formulation, preventing the need to extend the physical domain. Nonetheless, in Refs. 8), 9) and 10), a consistency analysis remains to be performed and has not yet been applied to incompressible formulations where the Poisson equation is solved.

This work is divided as follows: in §2, a continuous smoothed formulation of the involved differential operators and their corresponding consistency study is presented; in §3, the discrete versions of those differential operators in the presence of boundaries are formulated; in §4, the previous formulations are applied to the Poisson equation; in §5, different tests and examples are presented; in §6, a generalization to 2D is carried out; finally, in §7 two complex SPH problems are solved: a duct flow and a classical sloshing problem.

We should remark that the aim of this paper is to focus on the recovered consistency when boundary integral terms are included in the SPH formulation. For this reason, in §2 to §6, we will simplify some of the requirements that typically appear in SPH formulations (such as the symmetric properties of the gradient operator) and focus on the formulation consistency. In §7, where the boundary treatment is applied to complex problems, those typical symmetry requirements will be added and a detailed description of the treatment of each operator will be provided.

§2. Continuous smoothed formulation of differential operators

For the sake of clarity, all the analyses and most of the preliminary tests will be carried out in 1D; this simplifies the notation and the mathematical process; these ideas can be extended to 2D or 3D without any lack of generality. In order to present an immediate extension of these ideas to a 2D application, a Poisson problem is presented in §6.

Consider a bounded interval $(a, b) \subset \mathbb{R}$ and let $W_h(x)$ be a symmetric SPH

kernel defined on $\mathbb{R}$, such that

$$\int_{-\infty}^{\infty} W_h(y)dy = 1.$$

In order to simplify the technical details of our analysis, we shall assume that the kernel $W_h(x)$ vanishes for $|x| > 2h$. This assumption is fulfilled, for instance, when W_h is a Wendland-type kernel.[22)]

Let us define the Shepard normalization factor γ as

$$\gamma_h(x) := \int_a^b W_h(x-y)\,dy. \tag{2·1}$$

The SPH approximation with respect to the kernel W_h of a scalar function $p(x)$ on $\mathbb{R}$ taking real values is defined as

$$\langle p\rangle(x) := \frac{1}{\gamma_h(x)}\int_a^b p(y)\,W_h(x-y)\,dy. \tag{2·2}$$

The approximation defined in (2·2) is consistent, and its consistency can be expressed as

$$\langle p\rangle(x) = p(x) + \begin{cases} \mathcal{O}(h) & \text{for } x \text{ at a distance } \leq 2h \text{ from the boundary,} \\ \mathcal{O}\left(h^2\right) & \text{otherwise.} \end{cases} \tag{2·3}$$

Assuming that $4h < b-a$. Suppose that $x \in (a,b)$ is far from the boundary, i.e., $|x-a| > 2h$ and $|x-b| > 2h$. Then, $\gamma_h(x) = 1$ and, since the support of $W_h(x-\cdot)$ is contained in (a,b) one has

$$\langle p\rangle(x) = \int_{-\infty}^{\infty} p(y)\,W_h(x-y)\,dy; \tag{2·4}$$

therefore,

$$\langle p\rangle(x) - p(x) = \int_{-\infty}^{\infty} (p(y)-p(x))\,W_h(x-y)\,dy \tag{2·5}$$

$$= \int_{-\infty}^{\infty} \left(\frac{dp}{dx}(x)(y-x) + \mathcal{O}\left((x-y)^2\right)\right) W_h(x-y)\,dy \tag{2·6}$$

$$= \mathcal{O}\left(h^2\right); \tag{2·7}$$

using the property that, since W_h is symmetric, we have

$$\int_{-\infty}^{\infty} (y-x)\,W_h(x-y)\,dy = 0. \tag{2·8}$$

When x is at a distance less or equal to $2h$ from either a or b, it is not possible to exploit this cancellation property. If p is differentiable and x and y are in the support of W_h, then $|p(y)-p(x)| \leq C|y-x| \leq 2Ch$, where C is a constant. Therefore,

$$\langle p\rangle(x) - p(x) = \frac{1}{\gamma_h(x)}\int_a^b (p(y)-p(x))\,W_h(x-y)\,dy = \mathcal{O}(h). \tag{2·9}$$

It should be remarked that if the factor $1/\gamma_h$ is not present in Eq. (2·2), the obtained result would be similar to the one in Ref. 11), which is $\langle p\rangle(x) - p(x)/2 = \mathcal{O}(h)$.

2.1. *Approximation of the first-order derivative*

The SPH approximation of the first-order derivative dp/dx is set to be

$$\left\langle \frac{dp}{dx} \right\rangle (x) := \frac{1}{\gamma_h (x)} \int_a^b \frac{dp}{dx} (y) W_h (x-y)\, dy. \tag{2·10}$$

It follows that (see, for instance, Hu and Adams[23]), in the absence of a boundary (i.e., when $(a,b) = \mathbb{R}$), one has $\langle dp/dx \rangle (x) = dp/dx (x) + \mathcal{O}\left(h^2\right)$. Nonetheless, when boundaries are present, integrating by parts, we obtain

$$\left\langle \frac{dp}{dx} \right\rangle (x) = \frac{1}{\gamma_h (x)} \int_a^b p (y) W_h' (x-y)\, dy + \frac{1}{\gamma_h (x)} \left[p (b) W_h (x-b) - p (a) W_h (x-a) \right], \tag{2·11}$$

where $W_h' (s)$ stands for the derivative of the kernel with respect to s.

Again, this approximation is consistent:

$$\left\langle \frac{dp}{dx} \right\rangle (x) = \frac{dp}{dx} (x) + \begin{cases} \mathcal{O} (h) & \text{for } x \text{ at a distance } \leq 2h \text{ from the boundary,} \\ \mathcal{O}\left(h^2\right) & \text{otherwise.} \end{cases} \tag{2·12}$$

To check this identity, we proceed by following the ideas of the preceding section. While $4h < b-a$ and $x \in (a,b)$ at a distance from the boundary greater than $2h$, the contribution to Eq. (2·11) involving boundary terms vanishes. Moreover, since the support of the kernel is contained in the interval $(-2h, 2h)$, the integral in (2·11) can be extended to $\mathbb{R}$. This implies that expression (2·11) coincides with the usual SPH approximation of the gradient.

Suppose now $|x-b| \leq 2h$ (the analysis in the case $|x-a| \leq 2h$ is completely analogous); note that, in this case, $W_h (x-a) = 0$ and the following identity holds:

$$\frac{1}{\gamma_h (x)} p (b) W_h (x-b) = -\frac{1}{\gamma_h (x)} \int_a^b p (b) W_h' (x-y)\, dy. \tag{2·13}$$

Hence,

$$\left\langle \frac{dp}{dx} \right\rangle (x) = \frac{1}{\gamma_h (x)} \int_a^b (p (y) - p (b)) W_h' (x-y)\, dy \tag{2·14}$$

$$= \frac{1}{\gamma_h (x)} \int_a^b (p (y) - p (x) + p (x) - p (b)) W_h' (x-y)\, dy \tag{2·15}$$

$$= \frac{dp}{dx} (x) \frac{1}{\gamma_h (x)} \int_a^b (y-b) W_h^{'} (x-y) + \mathcal{O} (h) \tag{2·16}$$

$$= \frac{dp}{dx} (x) + \mathcal{O} (h). \tag{2·17}$$

As pointed out in Ref. 11), if a proper and consistent formulation is searched when a gradient is calculated near the boundary, the boundary terms cannot be neglected. In our case, the improvements are coming from the combination of the boundary terms and the normalization factor $1/\gamma_h$. We should also comment that although the consistency results are greatly improved with this formulation, if this expression

is used for pressure gradient calculations, an important drawback appears as the nonpreservation of linear momentum. This drawback could be fixed if a symmetrized formulation is used; see Ref. 11).

2.2. *Approximation of the second-order derivative*

We recall that the SPH approximation of the second-order derivative d^2p/dx^2 on $\mathbb{R}$ of a function $p(x)$ is defined as

$$\left\langle \frac{d^2p}{dx^2} \right\rangle (x) := \frac{1}{\gamma_h(x)} \int_a^b \frac{d^2p}{dx^2}(y) W_h(x-y) dy. \tag{2·18}$$

As proved by Español and Revenga,[24] again in the boundaryless case, $\left\langle d^2p/dx^2 \right\rangle (x) = d^2p/dx^2(x) + \mathcal{O}(h^2)$. When the fluid domain is limited by a boundary, we can again integrate by parts to obtain

$$\left\langle \frac{d^2p}{dx^2} \right\rangle (x) = \frac{1}{\gamma_h(x)} \int_a^b \frac{dp}{dx}(y) W_h'(x-y) dy + \frac{1}{\gamma_h(x)} \left[\frac{dp}{dx}(b) W_h(x-b) - \frac{dp}{dx}(a) W_h(x-a) \right]. \tag{2·19}$$

We propose the following discretization of the above formula:

$$\left\langle \frac{d^2p}{dx^2} \right\rangle (x) = \frac{2}{\gamma_h(x)} \left[\int_a^b \frac{p(y)-p(x)}{y-x} W_h'(x-y)\, dy + \frac{p(x)-p(b)}{x-b} W_h(x-b) - \frac{p(x)-p(a)}{x-a} W_h(x-a) \right]. \tag{2·20}$$

This formula is clearly exact if p is constant or linear. It turns out that it is also exact for $p(x) = x^2$:

$$\begin{aligned} \left\langle \frac{d^2p}{dx^2} \right\rangle (x) &= \frac{2}{\gamma_h(x)} \left[\int_a^b (y+x) W_h'(x-y)\, dy + (x+b) W_h(x-b) - (x+a) W_h(x-a) \right] \\ &= \frac{2}{\gamma_h(x)} \left[\int_a^b y W_h'(x-y)\, dy + b W_h(x-b) - a W_h(x-a) \right] \\ &= \frac{2}{\gamma_h(x)} \int_a^b W_h(x-y)\, dy \\ &= 2. \end{aligned}$$

More generally, formula (2·20) defines a consistent approximation to the second derivative:

$$\left\langle \frac{d^2p}{dx^2} \right\rangle (x) = \frac{d^2p}{dx^2}(x) + \begin{cases} \mathcal{O}(h) & \text{for } x \text{ at distance } \leq 2h \text{ of the boundary,} \\ \mathcal{O}(h^2) & \text{otherwise.} \end{cases} \tag{2·21}$$

Let h satisfy $4h < b-a$. In that case, if $|x-a| > 2h$ and $|x-b| > 2h$, then,

$$W_h(x-a) = W_h(x-b) = 0, \qquad \gamma_h(x) = 1, \tag{2·22}$$

and, therefore, the contribution of the boundary terms in the expression (2·20) also vanishes. This implies

$$\left\langle \frac{d^2p}{dx^2} \right\rangle (x) = 2 \int_a^b \frac{p(y)-p(x)}{y-x} W_h'(x-y)\, dy = 2 \int_{-\infty}^{+\infty} \frac{p(y)-p(x)}{y-x} W_h'(x-y)\, dy, \tag{2·23}$$

and the $\mathcal{O}\left(h^2\right)$ error term in formula (2·21) coincides with the analysis described in Ref. 24).

Therefore, it is sufficient to check (2·21) for the points $x \in [a,b]$ that are at a distance less or equal to $2h$ from the boundary of the interval. We shall assume in what follows that $|x-b| \leq 2h$, the analysis for the other boundary point a being completely analogous. The limited range assumption on the SPH kernel implies that $W_h(x-a) = 0$, and the finite difference appearing in the boundary term of (2·20) can be approximated by

$$\frac{p(x)-p(b)}{x-b} = \frac{dp}{dx}(x) + \frac{1}{2}\frac{d^2p}{dx^2}(x)(b-x) + \mathcal{O}\left(h^2\right). \tag{2·24}$$

Analogously, the integrand appearing in (2·20) can be expanded as

$$2\frac{p(y)-p(x)}{y-x} = 2\frac{dp}{dx}(x) + \frac{d^2p}{dx^2}(x)(y-x) + \mathcal{O}\left((x-y)^2\right). \tag{2·25}$$

Integrate the above formula against $\gamma_h^{-1}(x) W_h'(x-y)$ on $y \in (a,b)$. The left-hand side simply gives the expression of $\left\langle \frac{d^2p}{dx^2} \right\rangle (x)$ with the boundary terms removed. The terms on the right-hand side of (2·25) give the following contributions:

$$\frac{dp}{dx}(x)\frac{2}{\gamma_h(x)}\int_a^b W_h'(x-y)\,dy = -\frac{dp}{dx}(x)\frac{2}{\gamma_h(x)}W_h(x-b), \tag{2·26}$$

and

$$\frac{d^2p}{dx^2}(x)\frac{1}{\gamma_h(x)}\int_a^b (y-x)W_h'(x-y)\,dy = \frac{d^2p}{dx^2}(x)\left(1+\frac{(x-b)}{\gamma_h(x)}W_h(x-b)\right). \tag{2·27}$$

Therefore,

$$\begin{aligned}\left\langle \frac{d^2p}{dx^2} \right\rangle (x) = &-\frac{dp}{dx}(x)\frac{2}{\gamma_h}W_h(x-b) + \frac{d^2p}{dx^2}(x)\left(1+\frac{(x-b)}{\gamma_h(x)}W_h(x-b)\right) + \mathcal{O}(h)\\ &+\frac{2}{\gamma_h(x)}\left\{\frac{dp}{dx}(x) + \frac{1}{2}\frac{d^2p}{dx^2}(x)(b-x) + \mathcal{O}\left(h^2\right)\right\}W_h(x-b),\end{aligned} \tag{2·28}$$

and canceling terms, we conclude:

$$\left\langle \frac{d^2p}{dx^2} \right\rangle (x) = \frac{d^2p}{dx^2}(x) + \mathcal{O}(h). \tag{2·29}$$

Note that the fact that the order of consistency for x close to the boundary is smaller than the one obtained in the interior is due to the absence of cancellations (that take place in the boundaryless case, or in the interior) of second-degree terms in h in the expression (2·24).

As pointed out in Ref. 12), when a Laplacian is calculated near the boundary using typical SPH formulations, local inconsistencies might appear. In our case, the presence of boundary terms and the normalization factor $1/\gamma_h$ achieve local consistency.

§3. Discrete SPH formulation of differential operators

Now, we describe the discrete versions of the continuous SPH approximations of first and second derivatives introduced in the preceding section. Let us assume that we have a discretization $\{x_1, x_2, \ldots, x_N\}$ of (a, b) using N particles at these positions and that $x_1 = a$, $x_N = b$. We discretize the first-order derivative as

$$\left\langle \frac{dp}{dx} \right\rangle_m = \frac{1}{\gamma_m} \sum_n \frac{m_n}{\rho_n} p_n W_h'(x_m - x_n) + \frac{1}{\gamma_m} \left[p_b W_h(b - x_m) - p_a W_h(a - x_m) \right], \quad (3\cdot1)$$

where the subscript m is used for the particle studied and n for the neighboring particles. A detail worth mentioning is that the index n only affects the interior particles and excludes the boundary particles; this is $n \neq a$ and $n \neq b$. Each particle n possesses mass m_n, density ρ_n, position x_n, and the value of the function $p(x_n)$ is noted as p_n for that particle. We abuse the notation for p_1 and p_N, referring to them as p_a and p_b, respectively.

Regarding the second-order derivative, we define

$$\left\langle \frac{d^2p}{dx^2} \right\rangle_m = \frac{2}{\gamma_m} \left[\sum_n \frac{m_n}{\rho_n} \frac{p_m - p_n}{x_m - x_n} W_h'(x_m - x_n) + \frac{p_m - p_b}{x_m - x_b} W_h(b - x_m) - \frac{p_m - p_a}{x_m - x_a} W_h(a - x_m) \right], \quad (3\cdot2)$$

which is a particular one-dimensional version of the following expression introduced independently by Español and Revenga and Morris et al. in Refs. 24) and 25) respectively, in the absence of boundaries

$$\nabla^2 p_m \approx \frac{2}{\rho_m} \sum_n m_n \frac{p_{mn} \boldsymbol{x}_{mn} \cdot \nabla_{\boldsymbol{x}} W_h(\boldsymbol{x}_{mn})}{|\boldsymbol{x}_{mn}|^2}, \quad (3\cdot3)$$

where $p_{mn} = p_m - p_n$ and $\boldsymbol{x}_{mn} = \boldsymbol{x}_m - \boldsymbol{x}_n$.

§4. Discrete Poisson problem and boundary conditions

As introduced in §1, the solution of the incompressible Navier-Stokes system is commonly based on well-known techniques such as projection or fractional step methods.[16)–19)] These methodologies decouple velocity and pressure and the evolution of the Navier-Stokes system can be solved iterating simpler substeps per time step. Under the incompressibility assumption, in the second substep of the fractional step method, the following Poisson-type equation must be solved:

$$\nabla^2 p = \frac{\rho}{\Delta t} (\nabla \cdot \boldsymbol{u}^*), \quad (4\cdot1)$$

where ∇^2 stands for the Laplace operator, ρ is the density and Δt is the time step used in the temporal discretization.

This equation requires boundary conditions that are imposed on the boundary Γ of the fluid domain. Depending on the nature of the problem under consideration, different boundary conditions can be used; the most common ones being:

- *Dirichlet boundary conditions.* When free surface flows are involved in the calculation, the free surface is assumed to have a constant pressure equal to the gas that lies on the other side. In atmospheric flows, relative pressure is most commonly used and, consequently, the pressure boundary condition at the free surfaces Γ_F is $p = 0$.
- *Neumann boundary conditions.* These boundary conditions are usually employed to model a wall that constrains the expansion of the fluid. The boundary condition imposed on the boundary Γ_W is $\partial p/\partial n = 0$.

The Poisson problem we shall be dealing with can be described as follows: given a function $f(x)$, we wish to compute a function $p(x)$ that is a solution to the following problem:

$$-\nabla^2 p = f(x), \qquad x \in [a, b], \\ + \text{ Boundary Conditions.} \tag{4·2}$$

The discretization of the Laplacian involves the construction of a matrix that represents the operator. In our case, the matrix representing the Laplacian operator in 1D (left-hand side of Eq. (3·2)) can be explicitly found in the Appendix.

Once the matrix representation of the Laplacian operator has been constructed, boundary conditions should be implemented by suitably modifying the rows and columns of the matrix affected by these conditions. In 2D and 3D, the presence of a wall is implemented by the use of only one layer of boundary particles.

§5. Numerical results

5.1. *Consistency and numerical convergence*

We consider different basic problems in order to test the convergence of the method. The discretization of the Laplacian previously introduced corresponds to a consistent numerical approximation when

$$\Delta x \to 0, \tag{5·1}$$

$$h \to 0, \tag{5·2}$$

$$\Delta x/h \to 0, \tag{5·3}$$

and the solution obtained through our numerical approximation tends to the exact solution. In order to deal with the different situations that could appear in a fluid dynamic computation, we can distinguish between the direct and inverse problems. In the direct problem, the field p is given and the first and second derivatives are computed (this type of analysis falls under what is usually called *consistency* study); on the other hand, by inverse problem, we mean the problem of actually computing, for a given field f, the corresponding solution to the approximate equation through the inversion of a linear system that takes the boundary conditions into account. This is usually what *stability* and *convergence* analyses deal with.

5.1.1. Gradient computation

The simplest problem in this context is to consistently compute, for a given field $p(x)$, the first derivative in the interval $[a, b]$. Table I shows the maximum local

error (in L^∞ norm) obtained for the first-order derivative when expression (3·1) is used for different polynomial functions $p(x) = x^k, \quad k = 0, 1, 2$ in the interval $[a, b] = [-5/2, 5/2]$. For all the tests and problems presented in this work, the Wendland kernel[22] was used.

As can be observed in Table I, the method is fully consistent and, in the continuum limit, the accuracy of the computation increases.

5.1.2. Primitive computation

Let us now consider the problem:

$$-\frac{dp}{dx} = f(x), \qquad x \in [a, b], \tag{5·4}$$

$$p(a) = \lambda. \tag{5·5}$$

In contrast to the problem presented in 5.1.1, the $p(x)$ function is now an unknown field and $f(x)$ is a given function. This problem is well posed only if a Dirichlet boundary condition is used, whilst the solution is undetermined if a Neumann boundary condition is used. Using Eqs. (2·11) and (3·1) to represent the first derivative, we obtain the continuous SPH version of the problem (5·4):

$$\begin{aligned} &-\frac{1}{\gamma_h(x)}\left[\int_a^b p(y)W_h'(y-x)dy + p(b)W_h(b-x) - p(a)W_h(a-x)\right] \\ &=\frac{1}{\gamma_h(x)}\int_a^b f(y)W_h(y-x)dy. \end{aligned} \tag{5·6}$$

Analogously, the discrete version of this problem for a particle at $x = x_m$ is

$$\begin{aligned} &-\frac{1}{\gamma_m}\sum_n \frac{m_n}{\rho_n}p_n W_h'(x_m - x_n) - \frac{1}{\gamma_m}\left[p_b W_h(b - x_m) - p_a W_h(a - x_m)\right] \\ &=\frac{1}{\gamma_m}\sum_n f_n W_h(x_n - x_m). \end{aligned} \tag{5·7}$$

Given the values f_n, the values of p that satisfy problem (5·4) can be computed, writing Eq. (5·7) as a linear system:

$$A \cdot \begin{pmatrix} p_1 \\ p_2 \\ \vdots \\ p_N \end{pmatrix} = \begin{pmatrix} \frac{1}{\gamma_1}\sum_n f_n W_h(x_n - x_1) \\ \frac{1}{\gamma_2}\sum_n f_n W_h(x_n - x_2) \\ \vdots \\ \frac{1}{\gamma_N}\sum_n f_n W_h(x_n - x_N) \end{pmatrix}, \tag{5·8}$$

where A is the matrix that represents the gradient operator. To implement the boundary condition, we transform the matrix A into a new matrix A' with the same dimensions and whose first row is zero with the exception of the element $A(1, 1) = 1$.

Table I. Maximum errors obtained when the gradients (first derivatives in 1D) of the different functions $p(x) = \{1, x, x^2\}$ are calculated with the expression (3·1) in the interval $[a, b] = [-5/2, 5/2]$.

		1	x	x^2
$1/\Delta x$	$h/\Delta x$	$\max_m \lvert\nabla p_m\rvert$	$\max_m \lvert\nabla p_m - 1\rvert$	$\max_m \lvert\nabla p_m - 2x_m\rvert$
4^2	8	0.0049	0.0122	0.5929
6^2	12	0.0033	0.0081	0.3814
8^2	16	0.0024	0.0061	0.2809
16^2	32	0.0012	0.0031	0.1365
20^2	40	9.7656e-004	0.0024	0.1086
30^2	60	6.5104e-004	0.0016	0.0718

Table II. Maximum errors obtained when the problem given by Eqs. (5·4) and (5·5) is solved with $f(x) = 0, 1, x$ and $\lambda = 1$ in the interval $[a, b] = [-5/2, 5/2]$.

		$f(x) = 0$	$f(x) = 1$	$f(x) = x$
$1/\Delta x$	$h/\Delta x$	$\max_m \lvert p_m - 1\rvert$	$\max_m \lvert p_m - (-x - 3/2)\rvert$	$\max_m \lvert p_m - (-x^2/2 + 33/8)\rvert$
4^2	8	0.0207	0.0854	0.1230
6^2	12	0.0188	0.0663	0.0589
8^2	16	0.0177	0.0626	0.0389
16^2	32	0.0157	0.0608	0.0215
20^2	40	0.0153	0.0598	0.0190
30^2	60	0.0147	0.0581	0.0164

We also replace the first element of the right-hand side vector of Eq. (5·8) by λ in order to satisfy the boundary condition. Note that the addition of the boundary terms corrects the classical boundary errors coming from the incompleteness of the kernel.

Let us now solve the problem described by Eqs. (5·4) and (5·5) in the interval $[a, b] = [-5/2, 5/2]$ for three different polynomial functions $f(x) = 0, 1, x$ fixing the value $\lambda = 1$. For the functions $f(x) = 0$, $f(x) = 1$ and $f(x) = x$, the exact solutions of the problems are the constant function $p(x) = 1$, the linear function $p(x) = -x - 3/2$ and the quadratic function $p(x) = -x^2/2 + 33/8$, respectively. As we can observe in Table II, convergence is achieved as the parameters Δx and $\Delta x/h$ both tend to zero.

5.1.3. Laplacian computation

We now proceed to compute consistently the second derivative of a given field $p(x)$ in the interval $[a, b]$. Table III shows the L_∞-norm errors obtained using the expression (3·2) as an approximation to the second derivative for different functions $p(x) = x, x^2$ in the interval $[a, b] = [-5/2, 5/2]$.

As can be noticed, the method is also fully consistent and, in the continuum limit, the agreement accuracy of the obtained approximations to the exact Laplacian increases.

Table III. Maximum errors obtained when the Laplacians (second derivatives in 1D) of the different functions $p(x) = \{x, x^2\}$ are calculated with the expression (3·2) in the interval $[a, b] = [-5/2, 5/2]$.

		$p(x) = x$	$p(x) = x^2$
$1/\Delta x$	$h/\Delta x$	$\max_m \lvert\nabla^2 p_m\rvert$	$\max_m \lvert\nabla^2 p_m - 2\rvert$
4^2	8	0.0079	0.0400
6^2	12	0.0057	0.0285
8^2	16	0.0044	0.0221
16^2	32	0.0023	0.0116
20^2	40	0.0019	0.0094
30^2	60	0.0013	0.0063

5.1.4. Poisson problem

Next, we solve a one-dimensional Poisson problem, involving a second-order operator. More precisely, the problem we are interested in is the following:

$$-\frac{d^2p}{dx^2} = f(x) \qquad x \in [a, b], \tag{5·9}$$

$$p(a) = \lambda, \tag{5·10}$$

$$p(b) = \mu. \tag{5·11}$$

As usual, the goal is to compute the unknown field $p(x)$ for a given source term $f(x)$. For this early stage, we shall restrict ourselves to the case of Dirichlet boundary conditions. Later, similar results are obtained when one boundary condition is replaced by a Neumann type. Using Eqs. (2·11) and (3·1) to approximate the second-order derivative leads to the following continuous SPH version of the problem in the interval $[a, b]$:

$$\begin{aligned} -\frac{2}{\gamma_h(x)}\Bigg[&\int_a^b \frac{p(x') - p(x)}{x' - x} W_h'\left(x - x'\right) dx' \\ &+ \frac{p(x) - p(b)}{x - b} W_h(x - b) - \frac{p(x) - p(a)}{x - a} W_h(x - a)\Bigg] \\ &= \frac{1}{\gamma_h(x)} \int_a^b f(y) W_h(y - x) dy. \end{aligned} \tag{5·12}$$

The discrete counterpart for a particle at $x = x_m$ can be written as

$$\begin{aligned} -\frac{2}{\gamma_m}\Bigg[&\sum_n \frac{m_n}{\rho_n} \frac{p_m - p_n}{x_m - x_n} W_h'(x_m - x_n) \\ &+ \frac{p_m - p_b}{x_m - x_b} W_h(x_m - b) - \frac{p_m - p_a}{x_m - x_a} W_h(x_m - a)\Bigg] \\ &= \frac{1}{\gamma_m} \sum_n f_n W_h(x_n - x_m). \end{aligned} \tag{5·13}$$

Table IV. Maximum errors obtained when the problem given by Eqs. (5·9)–(5·11) is solved with $f(x) = 1$, $\lambda = 1$ and $\mu = 1$ in the interval $[a, b] = [-5/2, 5/2]$.

		$f(x) = 1 \quad \lambda = 1 \quad \mu = 1$
$1/\Delta x$	$h/\Delta x$	$\max_m \lvert p_m - (x^2/2 - 17/8)\rvert$
4^2	8	7.2300e-4
6^2	12	2.5175e-4
8^2	16	1.1380e-4
16^2	32	1.5631e-5
20^2	40	8.1440e-6
30^2	60	2.4683e-6

Writing Eq. (5·9) as a linear system, we have

$$B \cdot \begin{pmatrix} p_1 \\ p_2 \\ \vdots \\ p_N \end{pmatrix} = \begin{pmatrix} \dfrac{1}{\gamma_1} \displaystyle\sum_n f_n W_h(x_n - x_1) \\ \dfrac{1}{\gamma_2} \displaystyle\sum_n f_n W_h(x_n - x_2) \\ \vdots \\ \dfrac{1}{\gamma_N} \displaystyle\sum_n f_n W_h(x_n - x_N) \end{pmatrix}, \tag{5·14}$$

where B is the matrix representation of the Laplacian operator; see the Appendix for an explicit representation.

To implement the boundary condition, we transform matrix B into a new matrix B' with the same dimensions, whose first and last rows are zero with the exception of the elements $B(1,1) = 1$ and $B(N,N) = 1$. We also replace the first and last elements of the right-hand side vector by λ and μ.

Let us now solve the problem presented in (5·9)–(5·11) for two different cases. In the first case, $f(x) = 1$, $\lambda = 1$ and $\mu = 1$ in the interval $[a, b] = [-5/2, 5/2]$, and in the second case, $f(x) = \sin(x)$, $\lambda = 1$ and $\mu = -1$ in the interval $[a, b] = [\pi/2, 3\pi/2]$; the exact solutions of those problems are the functions $p(x) = x^2/2 - 17/8$ and $p(x) = \sin(x)$, respectively. As can be observed in Fig. 1, the presented agreement between the numerical and exact solutions is remarkable. We can also appreciate in Table IV that the consistency of the problem for the first case is fully achieved.

Let us now consider a particular problem where two different boundary conditions are used, one for each side of the domain. The problem can be formulated as

$$-\frac{d^2p}{dx^2} = x - \frac{1}{2}, \qquad x \in [0, 1], \tag{5·15}$$

$$p(x = a) = 0, \tag{5·16}$$

$$p'(x = b) = 0. \tag{5·17}$$

The exact solution to this problem in the interval $[a, b] = [0, 1]$ has the closed analytical form $p(x) = -x^3/6 + x^2/4$. We will show that the SPH discretization of this equation is able to approximate the analytical solution.

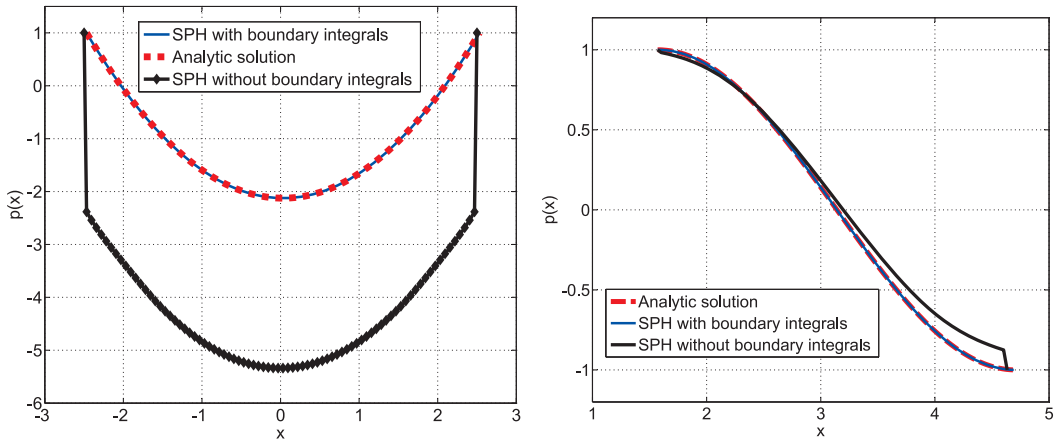

Fig. 1. Solution for the Dirichlet problem (5·9)–(5·11) when $f(x) = 1$(left) and $f(x) = \sin(x)$(right), $\Delta x = 1/4^2$ and $h = 1/2$

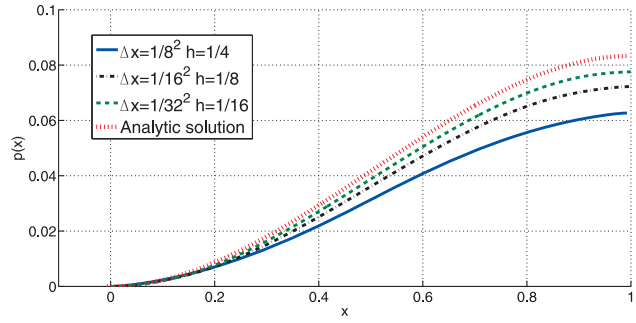

Fig. 2. Tendency towards the continuum for the Dirichlet-Neumann homogeneous case when $f = x - 1/2$.

Using the boundary condition $p'(x = b) = 0$, we can simplify Eq. (5·12) and thus obtain

$$\frac{-2}{\gamma_m}\sum_n \frac{m_n}{\rho_n}\frac{p_m - p_n}{x_m - x_n}W_h'(x_m - x_n) - \frac{2}{\gamma_m}\frac{p_m - p_a}{x_m - x_a}W_h(a - x_m) = \frac{1}{\gamma_m}\sum_n f_n W_h(x_n - x_m). \tag{5·18}$$

The analytical and different numerical approximations for the different discretization levels are plotted in Fig. 2. As can be observed, the numerical solution tends to the analytical solution when the parameters Δx and h tend to zero.

We should remark that if instead of using the boundary terms present in Eq. (5·18), the Dirichlet boundary condition were implemented extending the domain with few rows of dummy particles, strong inconsistencies $\mathcal{O}(1/h)$ and large discontinuities would be observed in the proximity of the boundaries (see Fig. 1, left). Several problems regarding the inconsistencies of extended domains are well documented in Ref. 21).

§6. 2D generalization

In this section, a typical 2D example has been included to show that the 2D extrapolation of the previous 1D formulation does not add further complications. Recalling the SPH approximation of the second derivative d^2p/dx^2 on $\mathbb{R}^2$ of a function $p(\boldsymbol{x})$:

$$\left\langle \nabla^2 p \right\rangle (\boldsymbol{x}) := \frac{1}{\gamma_h(\boldsymbol{x})} \int_\Omega \nabla^2_{\boldsymbol{y}} p(\boldsymbol{y}) W_h(\boldsymbol{x}-\boldsymbol{y}) d\boldsymbol{y}. \tag{6·1}$$

Integrating by parts the first term, we obtain

$$\begin{aligned}\left\langle \nabla^2 p \right\rangle (\boldsymbol{x}) = &\frac{1}{\gamma_h(\boldsymbol{x})} \int_\Omega \nabla_{\boldsymbol{y}} p(\boldsymbol{y}) \cdot \nabla_{\boldsymbol{x}} W_h(\boldsymbol{x}-\boldsymbol{y}) d\boldsymbol{y} \\ &+ \frac{1}{\gamma_h(\boldsymbol{x})} \int_\Gamma \left(\nabla_{\boldsymbol{y}} p(\boldsymbol{y}) \cdot \boldsymbol{n}_\Gamma(\boldsymbol{y})\right) W_h(\boldsymbol{x}-\boldsymbol{y}) d\boldsymbol{y},\end{aligned} \tag{6·2}$$

where $\boldsymbol{n}_\Gamma(\boldsymbol{y})$ is the unit *outward* normal vector to the boundary.

Equation (6·2) can be written as

$$\begin{aligned}\left\langle \nabla^2 p \right\rangle (\boldsymbol{x}) = &\frac{2}{\gamma_h(\boldsymbol{x})} \int_\Omega \left(p(\boldsymbol{y}) - p(\boldsymbol{x})\right) \frac{\boldsymbol{y}-\boldsymbol{x}}{|\boldsymbol{y}-\boldsymbol{x}|^2} \cdot \nabla W_h(\boldsymbol{x}-\boldsymbol{y})\, d\boldsymbol{y} \\ &+ \frac{2}{\gamma_h(\boldsymbol{x})} \int_\Gamma \left(p(\boldsymbol{y}) - p(\boldsymbol{x})\right) \frac{(\boldsymbol{y}-\boldsymbol{x}) \cdot \boldsymbol{n}_\Gamma}{|\boldsymbol{y}-\boldsymbol{x}|^2} W_h(\boldsymbol{x}-\boldsymbol{y})\, d\Gamma.\end{aligned} \tag{6·3}$$

The discrete version of Eq. (6·3) is therefore:

$$\begin{aligned}\left\langle \nabla^2 p \right\rangle_m = &\frac{2}{\gamma_m} \sum_n \frac{m_n}{\rho_n} (p_m - p_n) \frac{\boldsymbol{r}_m - \boldsymbol{r}_n}{|\boldsymbol{r}_m - \boldsymbol{r}_n|^2} \cdot \nabla W_h(\boldsymbol{r}_m - \boldsymbol{r}_n) \\ &+ \frac{2}{\gamma_m} \sum_n (p_m - p_n) \frac{(\boldsymbol{r}_m - \boldsymbol{r}_n) \cdot \boldsymbol{n}_\Gamma}{|\boldsymbol{r}_m - \boldsymbol{r}_n|^2} W_h(\boldsymbol{x}_m - \boldsymbol{x}_n)\, \Delta\Gamma,\end{aligned} \tag{6·4}$$

where $\Delta\Gamma$ is the distance between two consecutive boundary particles.

Let us apply expression (6·4) to the following problem:

$$\nabla^2 p = 2\left(\frac{\pi}{5}\right)^2 \sin\left(\frac{\pi x}{5} + \frac{\pi}{2}\right) \sin\left(\frac{\pi y}{5} + \frac{\pi}{2}\right) \quad x, y \in [-5/2, 5/2], \tag{6·5}$$

$$p(x = -5/2, y) = 0, \tag{6·6}$$

$$p(x = 5/2, y) = 0, \tag{6·7}$$

$$p(x, y = -5/2) = 0, \tag{6·8}$$

$$p(x, y = 5/2) = 0. \tag{6·9}$$

The problem (6·5)–(6·9) has $p(x,y) = -\sin(\pi(x/5 + 0.5))\sin(\pi(y/5 + 0.5))$ as an analytical solution. Three different sets of parameters were used for the computation ($\Delta x = 1/4, h = 1$), ($\Delta x = 1/9, h = 2/3$) and ($\Delta x = 1/16, h = 1/2$), and consistent results were once again obtained; see Table V. As an example, in Fig. 3, the complete solution for the case ($\Delta x = 1/4^2, h = 1/2$) is represented; furthermore, a cut of this solution by the plane $y = 0$ and the equivalent solution without boundary terms have been compared.

Table V. Maximum errors (L^∞ norm) obtained for the 2D Poisson problem (6·5)–(6·9).

$1/\Delta x$	$h/\Delta x$	$\max_m \lvert p_m + \sin(\pi(x/5+0.5))\sin(\pi(y/5+0.5))\rvert$
2^2	4	0.2327
3^2	6	0.1575
4^2	8	0.1180

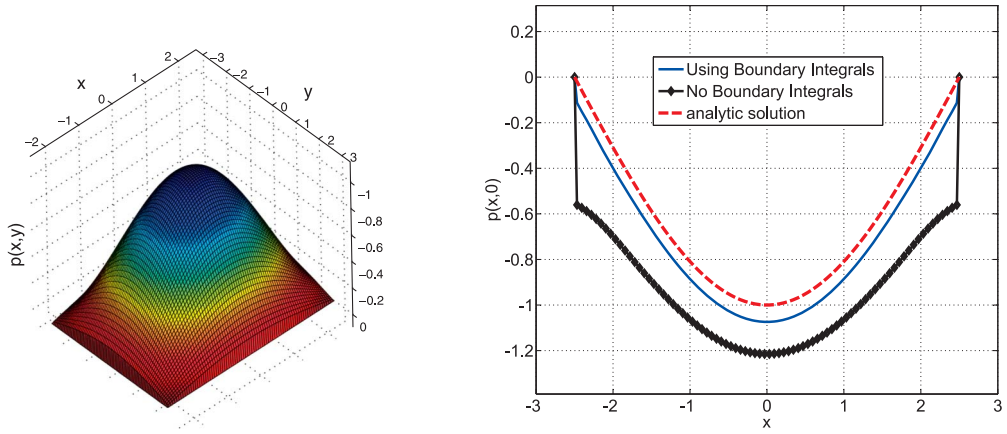

Fig. 3. Left: solution of the 2D Poisson problem (6·5)–(6·9), $\Delta x = 1/4^2$ and $h = 1/2$. Right: cut by a plane $y = 0$ of the solutions with and without the boundary terms.

§7. Practical applications

As was mentioned in the introduction and for the following practical applications, the WCSPH equations used will be the following:

1. mass conservation

$$\frac{d\rho_a}{dt} = -\frac{1}{\gamma_a}\left(\sum_b m_b \boldsymbol{v}_{ab}\cdot\nabla W_{ab} - \sum_s \rho_s \boldsymbol{v}_{as}\cdot\boldsymbol{n}_\Gamma W_{ab}\Delta\Gamma\right), \tag{7·1}$$

2. momentum conservation

$$\frac{d\boldsymbol{v}_a}{dt} = -\frac{1}{\gamma_a}\left[\sum_b m_b\left(\frac{p_a}{\rho_a^2}+\frac{p_b}{\rho_b^2}\right)\nabla W_{ab} - \sum_s \rho_s\left(\frac{p_a}{\rho_a^2}+\frac{p_b}{\rho_b^2}\right)\boldsymbol{n}_\Gamma W_{ab}\Delta\Gamma\right] + \boldsymbol{g}$$
$$+\frac{2\mu}{\gamma_a\rho_a}\left[\sum_b \frac{m_b}{\rho_b}\frac{\boldsymbol{v}_{ab}}{r_{ab}^2}\boldsymbol{r}_{ab}\cdot\nabla W_{ab} - \sum_s \boldsymbol{v}_{ab}\frac{\boldsymbol{r}_{ab}\cdot\boldsymbol{n}_\Gamma}{r_{ab}^2}W_{ab}\Delta\Gamma\right], \tag{7·2}$$

3. kinematics

$$\frac{d\boldsymbol{r}_a}{dt} = \boldsymbol{v}_a, \tag{7·3}$$

4. equation of state

$$p = \left(\frac{c^2\rho_0}{7}\right)\left(\left(\frac{\rho}{\rho_0}\right)^7 - 1\right), \tag{7·4}$$

where the subscript a refers to a generic fluid particle, subscript b is used for the neighboring fluid particles of particle a and subscript s is used for the neighboring boundary particles. The double subscript notation means $\boldsymbol{F}_{ab} = \boldsymbol{F}_a - \boldsymbol{F}_b$. The different terms in Eqs. (7·1)–(7·4) are as follows: $\boldsymbol{v}$ is the particle velocity, p is the pressure, $\boldsymbol{r}$ is the position vector, $\boldsymbol{n}_\Gamma$ is the unit inward normal vector to the boundary where the boundary particle s is situated, $\Delta\Gamma$ is the distance between boundary particles and t is time. Other parameters are as follows: $\boldsymbol{g}$ is gravity, μ is the dynamic viscosity of the fluid, c is the sound speed and ρ_0 is a reference density. During the following simulations, the density of the boundary particles ρ_s is interpolated from the fluid particles for every time step. A Wendland kernel has been used in the following simulations.

7.1. *Duct flow*

A stationary flow inside a square duct, driven by a constant pressure gradient along the axis of the duct (essentially a two-dimensional counterpart to plane Pouseuille flow) is now considered. The duct flow is a classical and paradigmatic example that points out the advantages of using a formulation where boundary conditions are consistently implemented for the velocity of the flow. This kind of computation is one of the first steps that has to be performed when a global stability analysis of a duct flow is computed; see Refs. 26) and 27).

A schematic representation of the domain is shown in Fig. 4 where a constant pressure gradient has been imposed along the z direction. The domain is defined as $(x, y) \in [-1, 1] \times [-1, 1]$. The constant pressure gradient drives a steady laminar flow that is independent of z and possesses a velocity vector $(0, 0, w)$ with a single component $w(x, y)$ along the z spatial direction. According to these hypotheses, Eqs. (7·1) and (7·2) can be reduced to the following Poisson equation:

$$\mu \nabla^2 w(x, y, t) = \nabla P, \tag{7·5}$$

where μ is the fluid viscosity and ∇P is the constant pressure gradient that drives

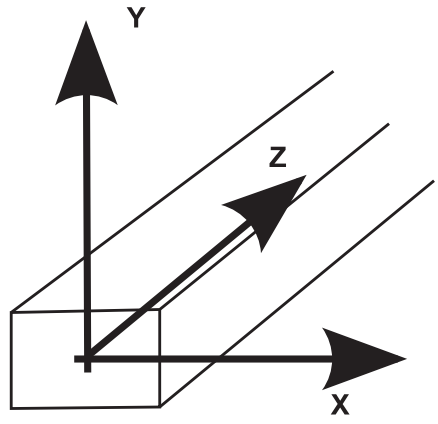

Fig. 4. Schematic representation of the duct flow problem.

the flow. The boundary conditions can be expressed as

$$\begin{aligned} w(x,-1) &= 0, \\ w(x,1) &= 0, \\ w(-1,y) &= 0, \\ w(1,y) &= 0. \end{aligned}$$

Taking $\nabla P/\mu = -2$, expression (7·5) can be written in SPH formalism as

$$\frac{2}{\gamma_a \rho_a}\left[\sum_b \frac{m_b}{\rho_b}\frac{w_{ab}}{r_{ab}^2}\boldsymbol{r}_{ab}\cdot\nabla W_{ab} - \sum_s w_{ab}\frac{\boldsymbol{r}_{ab}\cdot\boldsymbol{n}_\Gamma}{r_{ab}^2}W_{ab}\Delta\Gamma\right] = 2. \tag{7·6}$$

Since this case is a practical application, the convergence criteria has been adapted to typical industrial applications where the computational demands and the accuracy of the solution must be balanced. Systematic convergence procedures such as the ones shown in previous sections would increase the matrix size too much, leading to an excessive CPU time. The standard procedure is normally performed by increasing the number of particles $\Delta x \to 0$ while the ratio $h/\Delta x = 2$ is kept constant.

The solution obtained by the SPH approximation using boundary integrals has been compared with the equivalent solution obtained when a finite element method (FEM) is used. The number of nodes of the unstructured mesh used in the FEM calculation has been systematically increased until a final converged solution has been obtained. In this context, the FEM solution should be approximated by the SPH computations as the number of particles is increased, making Δx tend to zero.

Figure 5 shows the comparison between four different solutions for $\Delta x = 1/k^2$, $k = 6, 8, 10, 12$ and the FEM solution. As can be observed in Fig. 5, when the number of particles is increased, the SPH solution is able to approximate the reference FEM solution even in the vicinity of the boundary. The maximum error region can be found where the iso-contour lines have maximum separation.

In Fig. 6, the maximum velocity found at the middle point of the domain $(x, y) = (0, 0)$ is plotted for different values of k. Despite the convergence process not being as systematic as in the previous section where the three parameters h, $\Delta x/h$ and Δx were tending to zero, a noticeable tendency towards the solution given by FEM $\left(w_{max}^{FEM} = 0.5836\right)$ can be appreciated as the value of $k = 1/(\Delta x)^2$ increases.

7.2. *A 2D sloshing tank*

Since interest in the natural gas industry is increasing, the sloshing load is becoming a relevant research area, involving SPH as a simulation tool.[28] In this section, the results obtained when a sloshing phenomenon takes place in a rectangular tank are described. Experiment details (part of the SPHERIC benchmark*) are described by Botia-Vera et al.[29] In this article, lateral water impacts are experimentally measured with a pressure sensor. In Fig. 7, a schematic representation of the tank is shown. The water filling level for this experiment was $h = 93$ mm and the roll movement period was $T = 1.919$ around an axis placed at the middle point

*) http://wiki.manchester.ac.uk/spheric/index.php/Validation_Tests

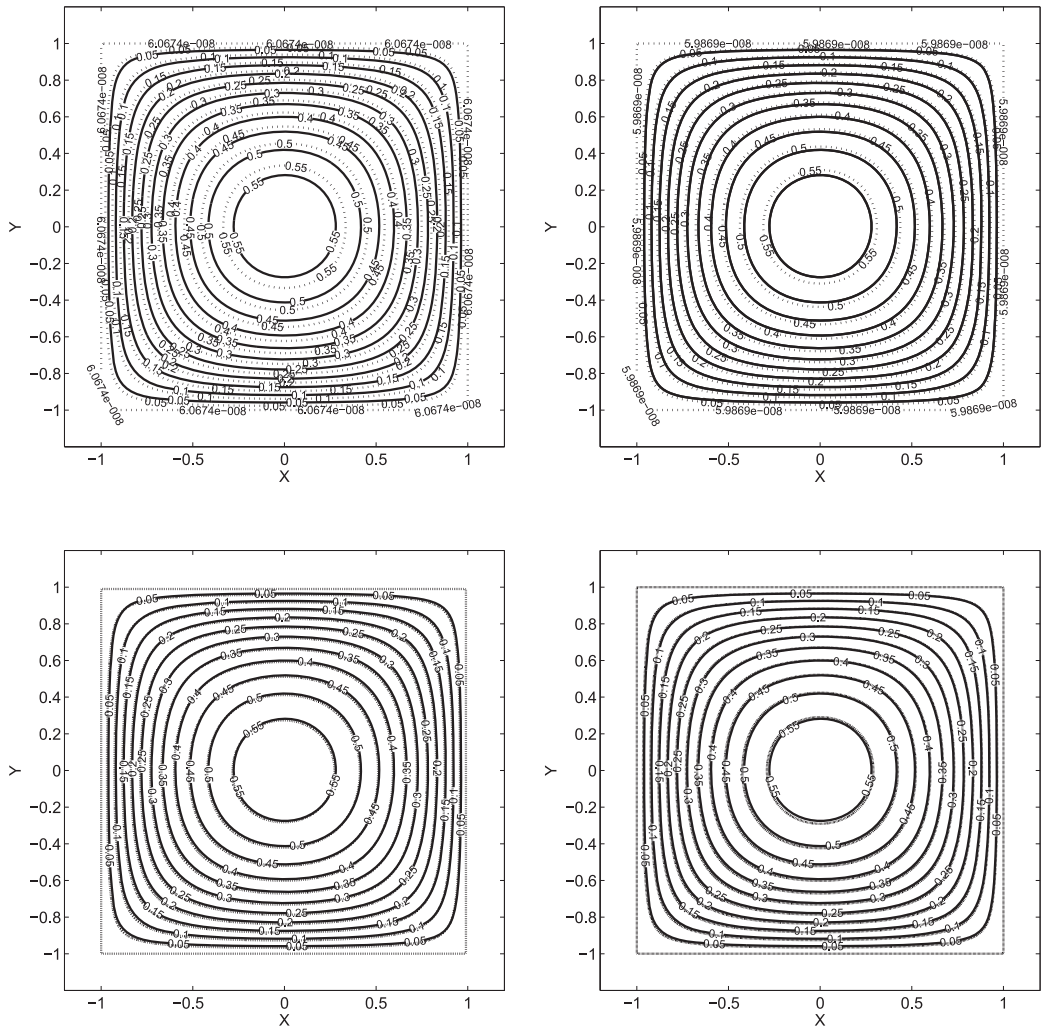

Fig. 5. Comparison between the SPH solution and FEM reference result for an increasing number of particles, $\Delta x = 1/k^2$, $k = 6$ (top left), $k = 8$ (top right), $k = 10$ (bottom left), $k = 12$ (bottom right).

of the bottom wall (red dot in Fig. 7). Pressure is measured for sensor 1; see Fig. 7. In our simulations, 148800 fluid particles were used, the artificial viscosity factor was $\alpha = 0.02$ and no periodic density reinitialization was considered. The value used for the sound speed in this problem was $c = 15\,\mathrm{m/s}$ following the literature recommendations,[28] and $\rho_0 = 998\,\mathrm{Kg/m^3}$ was used as reference fluid density.

In Fig. 8, the measured pressure for the first two wave impacts is shown. Owing to experimental repeatability difficulties,[30] the determination of the pressure peak value is extremely difficult, indicating that the comparison between experimental data and simulated results is adequately understood when qualitatively presented.

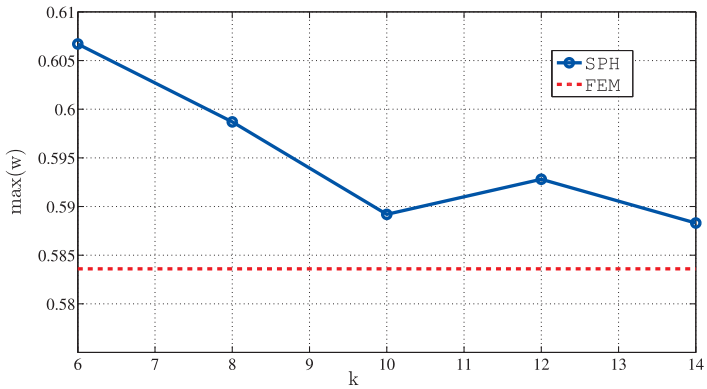

Fig. 6. Maximum value of $w(x, y)$ for an increasing number of particles, $\Delta x = 1/k^2$, $k = 6, 8, 10, 12, 14$. The maximum value of the reference FEM solution w_{max}^{FEM} is also plotted as a red line.

As can be observed, the average values of the SPH computations agree fairly well with the experimental measurements. In order to demonstrate the advantages of the boundary condition implementation presented in the previous sections of this work, our results have been compared with the ones presented by Delorme et al.[28] who used standard implementation of boundary conditions. From the different set of periods computed in Ref. 28), the most violent case, when the period is 0.9 times the natural frequency of the system, was selected for comparison. In Fig. 9, the measured pressures for the first wave impact are shown. As can be appreciated, introducing boundary conditions, as explained in the previous sections of the present work, greatly improves SPH results when compared with those of Delorme et al.[28]

Finally, in Fig. 10, a snapshot of the simulation corresponding to the moment when the pressure peak occurs, is represented. It can be seen that the numerical noise is restricted to the impact area and does not propagate to the whole domain. This is a significant progress over previous WCSPH implementations that do not consider boundary integrals (see, e.g. Ref. 20)).

§8. Conclusions

The inconsistencies coming from an inappropriate implementation of boundary conditions when SPH differential operators are discretized have been investigated. These inconsistencies clearly appear when studying the evolution of the solution as the discretization SPH parameters tend to the continuum. The inclusion of boundary terms that naturally appear in the formulation[9),10)] is implemented in order to solve the studied inconsistencies. The following conclusions were obtained:

1. In the smoothed continuum formulation, the inclusion of boundary integrals and normalization factors in 1D allows for a consistent $\mathcal{O}(h)$ formulation.
2. The corresponding discrete version with the inclusion of boundary integrals and normalization factors converges to the expected solution when the discretization

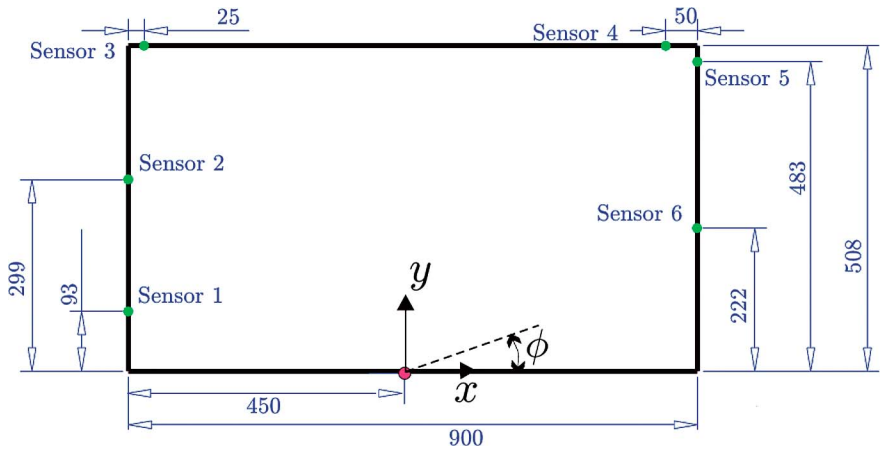

Fig. 7. Schematic view of the tank used. Dimensions are in mm.

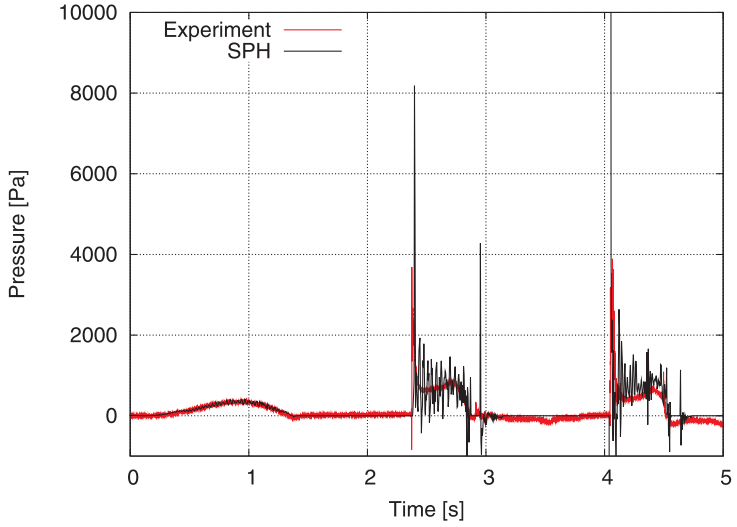

Fig. 8. Experimental and computational-SPH pressure evolution for sensor 1.

SPH parameters tend to zero.

3. Typical tests with the first and second derivative operators including a 2D Poisson problem and different practical applications confirm that this boundary condition implementation works consistently.

The overall conclusion is that the inclusion of both boundary terms and normalization factors in the SPH formulation is an appropriate method of implementing boundary conditions when consistent solutions of the fluid equations are desired.

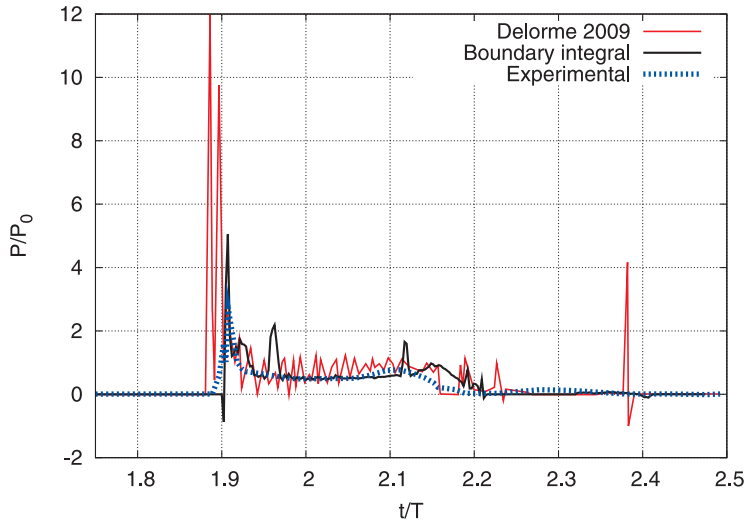

Fig. 9. Pressure evolution in sensor 1.

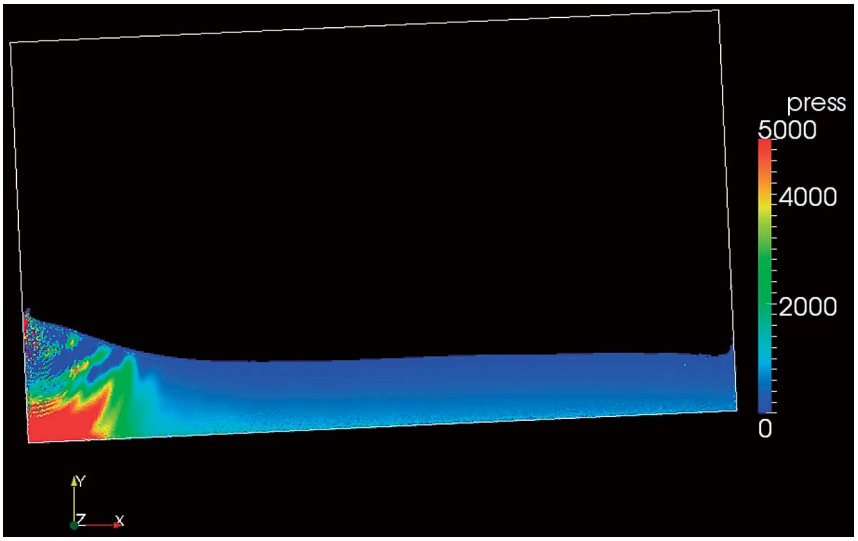

Fig. 10. Pressure field [Pa] at the pressure peak instant.

Acknowledgements

The research leading to these results has received funding from the Spanish Ministry for Science and Innovation under grant TRA2010-16988 *Caracterización Numérica y Experimental de las Cargas Fluido-Dinámicas en el transporte de Gas Licuado*. All the authors want to thank Mr. Hugo Gee for his valuable assistance during the preparation of this manuscript.

Appendix A
—— *Matrix Representation of the Laplacian Operator in 1D* ——

If a fluid particle m is closer than $2h$ from a fluid particle n and also from the left boundary particle a, the following terms must be included at the row matrix m:

$$B_{mm} = \frac{2}{\gamma_m}\left[\sum_n \frac{m_n}{\rho_n}\frac{W_h'(x_m - x_n)}{x_m - x_n} - \frac{W_h(a - x_m)}{x_m - x_a}\right], \tag{A·1}$$

$$B_{mn} = -\frac{2}{\gamma_m}\frac{m_n}{\rho_n}\frac{W_h'(x_m - x_n)}{x_m - x_n}, \tag{A·2}$$

$$B_{ma} = \frac{2}{\gamma_m}\frac{W_h(a - x_m)}{x_m - x_a}. \tag{A·3}$$

If a fluid particle m is closer than $2h$ from a fluid particle n and also from the right boundary particle b, the following terms must be included at the row matrix m:

$$B_{mm} = \frac{2}{\gamma_m}\left[\sum_n \frac{m_n}{\rho_n}\frac{W_h'(x_m - x_n)}{x_m - x_n} - \frac{W_h(b - x_m)}{x_m - x_b}\right], \tag{A·4}$$

$$B_{mn} = \frac{2}{\gamma_m}\frac{m_n}{\rho_n}\frac{W_h'(x_m - x_n)}{x_m - x_n}, \tag{A·5}$$

$$B_{mb} = -\frac{2}{\gamma_m}\frac{W_h(b - x_m)}{x_m - x_b}. \tag{A·6}$$

If a fluid particle m is closer than $2h$ from a fluid particle n and it is further than $2h$ from both boundaries:

$$B_{mm} = \frac{2}{\gamma_m}\sum_n \frac{m_n}{\rho_n}\frac{W_h'(x_m - x_n)}{x_m - x_n}, \tag{A·7}$$

$$B_{mn} = -\frac{2}{\gamma_m}\frac{m_n}{\rho_n}\frac{W_h'(x_m - x_n)}{x_m - x_n}. \tag{A·8}$$

References

1) J. J. Monaghan, Rep. Prog. Phys. **68** (2005), 1703.
2) A. Colagrossi and M. Landrini, J. Comput. Phys. **191** (2003), 448.
3) N. J. Quinlan, M. Lastiwka and M. Basa, Int. J. Numer. Methods Fluids **66** (2006), 2064.
4) A. Amicarelli, J. C. Marongiu, F. Leboeuf, J. Leduc, M. Neuhauser, L. Fang and J. Caro, Int. J. Numer. Methods Fluids **87** (2011), 677.
5) J. Bonet and M. X. Rodriguez-Paz, J. Comput. Phys. **209** (2005), 541.
6) J. J. Monaghan and J. B. Kajtar, Comput. Phys. Commun. **180** (2009), 1811.
7) T. Belytschko, Y. Krongauz, D. Organ, M. Fleming and P. Krysl, Comput. Methods Appl. Mech. Engrg. **139** (1996), 3.
8) M. Ferrand, D. Violeau, B. Rogers and D. Laurence, *Improved time scheme integration approach for dealing with semi-analytical wall boundary conditions in Spartacus2D* (5th International SPHERIC SPH Workshop, Manchester, 2010).
9) M. Ferrand, D. Violeau, B. Rogers and D. Laurence, *Consistent wall boundary treatment for laminar and turbulent flows in SPH* (6th International SPHERIC SPH Workshop, Hamburg, 2011).

10) M. Ferrand, D. R. Laurence, B. Rogers, D. Violeau and C. Kassiotis, Int. J. Numer. Methods Fluids, in press, only available on line, DOI: 10.1002/fld.3666 (2012).
11) A. Colagrossi, M. Antuono and D. Le Touzé, Phys. Rev. E **79** (2009), 056701.
12) A. Colagrossi, M. Antuono, A. Souto-Iglesias and D. Le Touzé, Phys. Rev. E **84** (2011), 026705.
13) F. Macià, J. M. Sánchez, A. Souto-Iglesias and L. M. González, Int. J. Numer. Methods Fluids **69** (2012), 509.
14) S. J. Cummins and M. Rudman, J. Comput. Phys. **152** (1999), 584.
15) S. Koshizuka, Y. Oka and H. Tamako, *A particle method for calculating splashing of incompressible viscous fluid* (Int. Conf. Mathematics and Computations, Reactor Physics, and Environmental Analyses, La Grange Park, IL, 1995).
16) J. Kim and P. Moin, J. Comput. Phys. **59** (1985), 308.
17) R. Temam, Bull. Soc. Math. France **98** (1968), 115.
18) J. B. Perot, J. Comput. Phys. **108** (1993), 51.
19) A. J. Chorin, Math. Comp. **22** (1968), 745.
20) E. S. Lee, C. Moulinec, R. Xu, D. Violeau, D. Laurence and P. Stansby, J. Comput. Phys. **227** (2008), 8417.
21) F. Macià, M. Antuono, M. L. M. González and A. Colagrossi, Prog. Theor. Phys. **125** (2011), 1091.
22) H. Wendland, Adv. in Comput. Math. **4** (1995), 389.
23) X. Y. Hu and N. A. Adams, Phys. of Fl. **18** (2006), 702.
24) P. Español and M. Revenga, Phys. Rev. E **67** (2003), 026705.
25) J. P. Morris, P. J. Fox and Y. Zhu, J. Comput. Phys. **136** (1997), 214.
26) T. Tatsumi and T. Yoshimura, J. Fluid. Mech. **212** (1990), 437.
27) V. Theofilis, P. W. Duck and J. Owen, J. Fluid. Mech. **505** (2004), 249.
28) L. Delorme, A. Colagrossi, A. Souto-Iglesias, R. Zamora-Rodriguez and E. Botia-Vera, Ocean Eng. **36** (2009), 168.
29) E. Botia-Vera, A. Souto-Iglesias, G. Bulian and L. Lobovský, *Three SPH Novel Benchmark Test Cases for free surface flows* (5th International SPHERIC SPH Workshop, Manchester, 2010).
30) A. Souto-Iglesias, E. Botia-Vera and G. Bulian, *Repeatability and Two-Dimensionality of Model Scale Sloshing Impacts* (5th 22nd Int. Offshore and Polar Engineering Conf. (ISOPE), Rhodes, 2012).